INTERNATIONAL JOURNAL FOR NUMERICAL METHODS IN FLUIDS
Int. J. Numer. Meth. Fluids 2009; **59**:405–421
Published online 28 April 2008 in Wiley InterScience (www.interscience.wiley.com). DOI: 10.1002/fld.1822

A lattice Boltzmann-BGK algorithm for a diffusion equation with Robin boundary condition—application to NMR relaxation

A. Hiorth[1,*,†], U. H. a Lad[2], S. Evje[1] and S. M. Skjæveland[2]

[1]*IRIS-International Research Institute of Stavanger, P.O. Box 8046, N-4068 Stavanger, Norway*
[2]*Petroleum Department, University of Stavanger, N-4036 Stavanger, Norway*

SUMMARY

We present a lattice Boltzmann-BGK (LBGK) algorithm for a diffusion equation together with a Robin boundary condition, which we apply in the case of nuclear magnetic resonance relaxation. The boundary condition we employ is independent of the direction of the wall. This makes the algorithm very suitable for complicated geometries, such as porous media. We discuss the effect of lattice topology by using, respectively, an eight-speed and a four-speed lattice. The numerical algorithm is compared with analytical results for a square and an equilateral triangle. The eight-speed lattice performs well in both cases. The four-speed lattice performs well for the square, but fails in the case of an equilateral triangle. Comparison with a random walk algorithm is also included. The LBGK algorithm presented here can also be used for a convective diffusion problem if the speed of the fluid can be neglected close to the boundary. Copyright © 2008 John Wiley & Sons, Ltd.

Received 16 April 2007; Revised 20 December 2007; Accepted 8 March 2008

KEY WORDS: lattice Boltzmann; LBGK; NMR; Robin boundary condition; diffusion; relaxation

1. INTRODUCTION

We will present a lattice Boltzmann-BGK (LBGK) algorithm for a diffusion equation with a Robin boundary condition. This equation describes diffusion of a scalar field; the scalar field may represent energy, a chemical component or magnetization. Our focus will mainly be on application

*Correspondence to: A. Hiorth, IRIS-International Research Institute of Stavanger, P.O. Box 8046, N-4068 Stavanger, Norway.
†E-mail: aksel.hiorth@iris.no, ah@iris.no

Contract/grant sponsor: ConocoPhillips and the Ekofisk Coventurers
Contract/grant sponsor: TOTAL
Contract/grant sponsor: ENI
Contract/grant sponsor: Hydro
Contract/grant sponsor: Statoil
Contract/grant sponsor: Petoro

for nuclear magnetic resonance (NMR) relaxation. Although magnetic resonance is a quantum mechanical phenomenon, it can be described in terms of classical mechanics [1, 2]. In NMR experiments, an external field is applied to, for example, a fluid. The protons in the fluid will interact with the external field and because of thermal motion some protons will have their spin parallel to the external field and some anti-parallel. The protons with their spin parallel to the external magnetic field will have the lowest energy. The thermal motion will make the number of spins in the low energy state slightly higher than the high energy state. This results in a net magnetization from the fluid, which can be observed. By experimental methods, this magnetization can be flipped into the xy-plane. The characteristic time it takes for the z-component to disappear from the xy-plane is called T_2 (spin–spin relaxation) and the characteristic time it takes to reach thermal equilibrium is called T_1 (spin–lattice relaxation).

During relaxation, if the spins are constrained by some kind of geometry, this will make the magnetic signal disappear faster. The interaction of spins with the surface is modeled as a diffusion equation with a Robin boundary condition [1, 2]. From a mathematical point of view, there is no difference between relaxing spin and absorption of a diffusing chemical component in a solute. In NMR one is normally interested in the total concentration in the solute or the number of spins 'alive,' as this can be measured as the magnetic signal from the sample.

The traditional approach to calculate the NMR signal has been random walk (RW) [3–8]. Lattice Boltzmann (LB) algorithms for a convective diffusion equation have been used in the case of heat conduction [9–13] and in the case of adsorption of chemical components [14–17]. To our knowledge, there have been no attempts applying a LB algorithm to NMR relaxation. We compare numerical solutions with corresponding analytical solutions for a square and an equilateral triangle. We also discuss the effect of the number of velocity vectors used for calculating the numerical solution via the LBGK method. It turns out that the Robin boundary condition is very sensitive to the discretization of the boundary. In particular, we observe that the eight-speed lattice gives results that are much better than the four-speed lattice for the case with the equilateral triangle. The four velocity lattice produces wrong solutions, due to inappropriate representation of the boundary. We also make a comparison between the RW algorithm and the LB algorithm on a square domain.

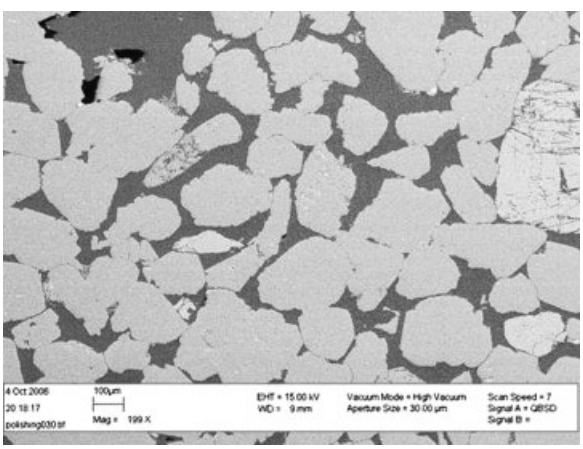

Figure 1. An SEM image of a thin section of a sandstone core. The total length of the image is 2 mm.

DOI: 10.1002/fld

Our result reflects that the LB algorithm is more accurate at a low number of grid points; this is partly a consequence of the stochastic nature of RW.

The boundary condition presented in this paper is shown to be related to the same type of boundary condition used in RW simulations of NMR relaxation [3–8]. A nice feature then is that the boundary condition is independent of the orientation of the wall. This makes the proposed algorithm well suited for application to irregular geometries such as porous media. As an illustration of the complexity of a porous medium, there is a scanning electron image (SEM) of a thin section of a sandstone core in Figure 1.

The outline of the article is as follows: in Section 2 we derive the convective diffusion equation by the use of a Chapman–Enskog expansion. In Section 3 we present the boundary condition in the limit of zero flow velocity. Further, in Section 3 we compare the numerical and analytical solution for a square and an equilateral triangle. We also include a comparison between RW and LB. Finally, in Section 4 we present discussion and conclusions.

2. THE LB METHOD

The LB is a mesoscopic particle-based approach to simulate a physical system. Fictitious particles move on a regular lattice and collide with each other. A collision rule is obeyed for particles meeting at the same lattice point or neighbor points for multi-phase problems [18].

In this work, we assume that we have one type of species that represents a component dissolved in a fluid flowing with a velocity $\mathbf{u}$. This component may be the concentration of a chemical component or the density of magnetic spin. The component may react with the wall and obey the following equation in the interior of the fluid:

$$f_i(\mathbf{x}+\mathbf{c}_i\delta_t, t+\delta_t) - f_i(\mathbf{x},t) = -\frac{1}{\tau}[f_i(\mathbf{x},t) - f_i^{\mathrm{eq}}(\mathbf{x},t)] \tag{1}$$

where $f_i(\mathbf{x},t)$ represents the distribution of particles entering site $\mathbf{x}$ at time t and moving in the direction i with velocity $\mathbf{c}_i$. The right-hand side of Equation (1) represents the collision operator and all the directions relax with a single relaxation time τ. The collision operator is simply the difference between the local equilibrium solution $f_i^{\mathrm{eq}}(\mathbf{x},t)$ and the distribution function. The lattice topology satisfies the following relations [19]:

$$\begin{aligned} \sum_i^N \omega_i &= 1 \\ \sum_i^N \omega_i c_{i\alpha} &= 0 \\ \sum_i^N \omega_i c_{i\alpha} c_{i\beta} &= C_2 c^2 \delta_{\alpha,\beta} \\ \sum_i^N \omega_i c_{i\alpha} c_{i\beta} c_{i\gamma} &= 0 \end{aligned} \tag{2}$$

where the Greek indices go over the spatial dimensions and the Latin indices go over the number of velocity vectors. $c = \delta_x/\delta_t$ is the speed of sound on the lattice, and ω_i are the weights and can be

DOI: 10.1002/fld

assumed as the mass of a particle moving in the i direction. The form of the equilibrium distribution function $f_i^{\mathrm{eq}}(\mathbf{x},t)$ determines the continuum equations. In order to describe a convective diffusion process, we choose the following form [9]:

$$f_i^{\mathrm{eq}}(\mathbf{x},t)=\omega_i\rho\left[1+\frac{1}{C_2}\frac{\mathbf{c}_i\cdot\mathbf{u}}{c^2}\right] \tag{3}$$

where ρ represents the scalar field in this case the magnetic field and C_2 is the constant appearing in (2). The distribution function obey the following conservation laws:

$$\begin{aligned}\sum_i^N f_i(\mathbf{x},t)&=\rho(\mathbf{x},t)\\ \sum_i^N \mathbf{c}_i f_i(\mathbf{x},t)&=\rho(\mathbf{x},t)\mathbf{u}\end{aligned} \tag{4}$$

The continuum equations can be obtained by performing a Chapman–Enskog expansion. By assuming that δ_t is small, we can Taylor expand Equation (1):

$$\delta_t(\partial_t+\mathbf{c}_i\cdot\nabla)f_i(\mathbf{x},t)+\frac{\delta_t^2}{2}(\partial_t+\mathbf{c}_i\cdot\nabla)^2 f_i(\mathbf{x},t)+\mathcal{O}(\delta_t^3)=-\frac{1}{\tau}[f_i(\mathbf{x},t)-f_i^{\mathrm{eq}}(\mathbf{x},t)] \tag{5}$$

We then expand the distribution function and introduce two time scales, $t_0=t$ and $t_1=\delta_t t$:

$$\begin{aligned}f_i(\mathbf{x},t)&=f_i^{(0)}(\mathbf{x},t)+\delta_t f_i^{(1)}(\mathbf{x},t)+\delta_t^2 f_i^{(2)}(\mathbf{x},t)+\mathcal{O}(\delta_t^3)\\ \partial_t&=\partial_{t_0}+\delta_t\partial_{t_1}\end{aligned} \tag{6}$$

Substituting this equation into (5), we find to order $\mathcal{O}(\delta_t^3)$:

$$f_i^{(0)}(\mathbf{x},t)=f_i^{\mathrm{eq}}(\mathbf{x},t) \tag{7}$$

$$(\partial_{t_0}+\mathbf{c}_i\cdot\nabla)f_i^{(0)}(\mathbf{x},t)=-\frac{1}{\tau}f_i^{(1)}(\mathbf{x},t) \tag{8}$$

$$\partial_{t_1}f_i^{(0)}(\mathbf{x},t)+\left(1-\frac{1}{2\tau}\right)(\partial_{t_0}+\mathbf{c}_i\cdot\nabla)f_i^{(1)}(\mathbf{x},t)=-\frac{1}{\tau}f_i^{(2)}(\mathbf{x},t) \tag{9}$$

Multiplying Equations (8) and (9) with ω_i and taking the sum over i, we find

$$\partial_{t_0}\rho+\nabla\cdot(\rho\mathbf{u})=0 \tag{10}$$

$$\partial_{t_1}\rho+\left(1-\frac{1}{2\tau}\right)\sum_i^N\omega_i\nabla\cdot\mathbf{c}_i f_i^{(1)}=0 \tag{11}$$

where we have used Equations (2) and (7). We then multiply Equation (8) with $\mathbf{c}_i$ and sum over i:

$$\begin{aligned}\sum_i\omega_i\mathbf{c}_i f_i^{(1)}&=-\tau\sum_i(\partial_{t_0}+\mathbf{c}_i\cdot\nabla)\mathbf{c}_i f_i^{(0)}\\ &=-\tau(\partial_{t_0}(\rho\mathbf{u})+c^2C_2\nabla\rho)\end{aligned} \tag{12}$$

DOI: 10.1002/fld

Multiplying Equation (11) with δ_t, adding Equation (10) and inserting Equation (12), we find

$$(\partial_{t_0}+\delta_t\partial_{t_1})\rho+\nabla\cdot(\rho\mathbf{u})-C_2\left(\tau-\frac{1}{2}\right)\frac{\delta_x^2}{\delta_t}\nabla^2\rho-\left(\tau-\frac{1}{2}\right)\delta_t\nabla\cdot\partial_{t_0}(\rho\mathbf{u})=0 \tag{13}$$

The last term is formally of higher order as we consider fluids with small flow velocities, that is, $\mathbf{u}\sim\mathcal{O}(\delta_t)$. Then we finally arrive at the convective diffusion equation:

$$\begin{gathered}\partial_t\rho+\nabla\cdot(\rho\mathbf{u})-D\nabla^2\rho=0\\ D\equiv C_2\left(\tau-\frac{1}{2}\right)\frac{\delta_x^2}{\delta_t}\end{gathered} \tag{14}$$

In the remainder of this paper we will restrict ourselves to the case of no flow, i.e. $\mathbf{u}=0$.

3. METHOD OF COMPUTATION

We have not used any information about the particle velocity $\mathbf{c}_i$ and the weights ω_i apart from the constraints in Equation (2). As stated [20], if 90° rotational invariance is sufficient to yield full isotropy for diffusive phenomena, then the simplest representation of the equilibrium function would be to have a square lattice with four velocities [11, 20]. Other models have also been used [14–17]. We will use one model with four directions ($2DQ5$) and another with eight directions ($2DQ9$); see Figure 2. The velocity vectors will then be

$$\begin{aligned}[\mathbf{c}_1,\mathbf{c}_2,\mathbf{c}_3,\mathbf{c}_4,\mathbf{c}_5,\mathbf{c}_6,\mathbf{c}_7,\mathbf{c}_8]&=\begin{bmatrix}1&0&-1&0&1&-1&-1&1\\0&1&0&-1&1&1&-1&-1\end{bmatrix}\\ [\mathbf{c}_1,\mathbf{c}_2,\mathbf{c}_3,\mathbf{c}_4]&=\begin{bmatrix}1&0&-1&0\\0&1&0&-1\end{bmatrix}\end{aligned} \tag{15}$$

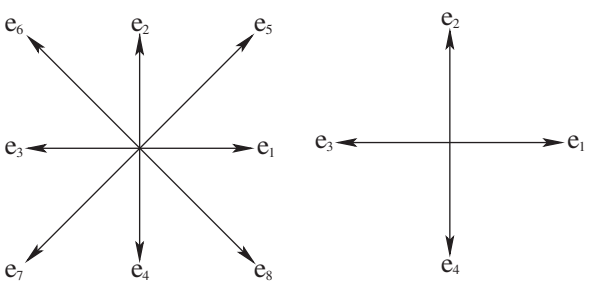

Figure 2. Velocities used in the LB algorithm. Left: eight velocities—$2DQ9$ and right: four velocities—$2DQ5$.

DOI: 10.1002/fld

All the weights will be chosen to be equal $\omega_i = \omega = \frac{1}{8}(2DQ9)$, $\frac{1}{4}(2DQ5)$. By inserting Equation (15) in the third relation of Equation (2) it follows that $C_2 = \frac{3}{4}(2DQ9)$, $\frac{1}{2}(2DQ5)$. Assuming the fluid to be stationary, it follows from (3) that we have the following equilibrium function:

$$f_i^{\mathrm{eq}}(\mathbf{x}, t) = \omega\rho(\mathbf{x}, t) \tag{16}$$

3.1. Implementation of the boundary condition

In LB implementation, the boundary condition reduces to the problem of expressing the (unknown) incoming distribution functions in terms of the (known) outgoing distributions functions. This problem is ill posed; there are several ways in which this can be done. We will justify the boundary conditions derived in this paper by comparison with analytical solutions. The continuum boundary condition is a Robin type of the form:

$$D\,\mathbf{n}\cdot\nabla\rho(\mathbf{x}, t) + \sigma(\mathbf{x})\rho(\mathbf{x}, t)|_{\mathscr{S}} = 0 \tag{17}$$

where σ is the surface relaxtivity. It is a measure of how strongly the spins interact with the surface or how strongly a chemical component adsorb to a surface. If $\sigma \to 0$ the spins just bounce back from the surface and if $\sigma \to \infty$ the spin hitting the surface 'dies,' that is, it does not contribute to the magnetic signal.

Our approach is motivated from the Chapman–Engskog expansion outlined in the previous section. Starting with Equation (8),

$$\mathbf{c}_i \cdot \nabla f_i^{\mathrm{eq}}(\mathbf{x}, t) = -\frac{1}{\tau} f_i^{(1)}(\mathbf{x}, t) \tag{18}$$

where we have used Equation (7) and assumed a steady state at the surface.[‡] On the basis of Equation (18), one may argue that the non-equilibrium part of the distribution function, $\delta_t f_i^{(1)} = f_i - f_i^{(\mathrm{eq})} + \mathscr{O}(\delta_t^2)$, is proportional to the concentration gradient dotted with the microscopic velocity at the surface [12–17]; hence, we can make the following assumption:

$$\mathbf{c}_i \cdot \nabla f_i^{\mathrm{eq}}(\mathbf{x}, t) = -\frac{C_2\, c}{D}(f_i(\mathbf{x}, t) - f_i^{\mathrm{eq}}(\mathbf{x}, t)) \tag{19}$$

The factor on the right-hand side will be justified by comparison with analytical solutions. Substituting (16) into Equation (19) and using (17), we find for a wall parallel to the y-axis:

$$\rho(\mathbf{x}, t) = \frac{f_1}{\omega + \omega\hat{\sigma}/C_2} \tag{20}$$

where $\hat{\sigma} \equiv \sigma\delta_t/\delta_x$ is a dimensionless parameter. By demanding a detailed balance, in the sense that the non-equilibrium part of the incoming distribution function equals the outgoing with opposite sign, we find

$$f_3 - f_3^{\mathrm{eq}} = -(f_1 - f_1^{\mathrm{eq}}) \tag{21}$$

[‡]The steady-state assumption is also used in Equation (17).

DOI: 10.1002/fld

which implies that

$$f_3 = (\zeta - 1) f_1, \quad \zeta \equiv \frac{2}{1 + \hat{\sigma}/C_2} \tag{22}$$

In the case of the $2DQ9$ lattice, we have two more distribution functions:

$$\begin{aligned} f_7 &= (\zeta - 1) f_5 \\ f_6 &= (\zeta - 1) f_8 \end{aligned} \tag{23}$$

Note that ζ is independent of the direction; this is a consequence of the fact that we have chosen all the weights equal, $\omega_i = \omega$. Having ζ independent of the direction makes this algorithm very easy to implement in irregular geometries. Assuming $\hat{\sigma}$ to be small,

$$\zeta \equiv \frac{2}{1 + \hat{\sigma}/C_2} \simeq 2 - \frac{2}{C_2}\hat{\sigma} \;\Rightarrow\; f_{\text{incoming}} = \left(1 - \frac{2}{C_2}\hat{\sigma}\right) f_{\text{outgoing}} \tag{24}$$

Comparing (22), (23) and (24), we see that the physical interpretation of the boundary condition is that only a part of the distribution function is reflected. That is, some of the spins have a probability of $2\hat{\sigma}/C_2$ of dying when hitting the wall; this is exactly the same type of boundary condition used in RW simulations of NMR [3–8].

3.2. Test of the boundary condition for a square

When performing the simulations with the LB algorithm, we place the boundaries half way between the lattice points instead of at the lattice points. This greatly improves the convergence to the analytical solutions, both in the case of the square and the triangle. This fact is illustrated in Figure 3. The left figure in Figure 3 shows the two solutions for a fixed time t_1, where $\rho(t_1)/\rho(0) \simeq 0.50$ and the figure clearly demonstrates that they are different close to the boundary. Comparison with the analytical solution (A15) (see Appendix A) reveals that placing the boundary half way between grid points gives the best result. In the right figure, we have plotted the magnetic signal as a function of time, and it is observed that the solution with the boundary half way between the grid points is very close to the analytical solution (A16).

Now, we will focus on a comparison between $2DQ5$ and $2DQ9$ lattice. We calculate the L_2 norm,

$$L_2 = \frac{\sqrt{\sum_i (\rho_N(x_i, y_i, t_1) - \rho(x_i, y_i, t_1))^2}}{\sqrt{\sum_i (\rho(x_i, y_i, t_1))^2}} \tag{25}$$

in the case of intermediate surface effects ($\gamma = 1$) and strong surface effects ($\gamma = 10$). Here $\rho_N(x_i, y_i, t_1)$ is the magnetic signal at a time $t = t_1$ for a given side length, $L = N\delta_x$, where N is the number of links. The time t_1 is chosen such that the magnetic signal is approximately 50% of its original value. $\rho(x_i, y_i, t_1)$ is the analytical solution; see Equation (A15). The surface effect can conveniently be summarized by the dimensionless parameter $\gamma = \sigma L/D$. L is a typical length scale, taken to be the length of one of the sides in the square or the triangle. If $\gamma \to \infty$, the Robin boundary condition reduces to a Dirichlet boundary condition $\rho(x, y, t)|_S = 0$ and if $\gamma \to 0$, the Robin boundary condition reduces to a Neumann boundary condition $n \cdot \nabla \rho(x, y, t)|_S = 0$.

DOI: 10.1002/fld

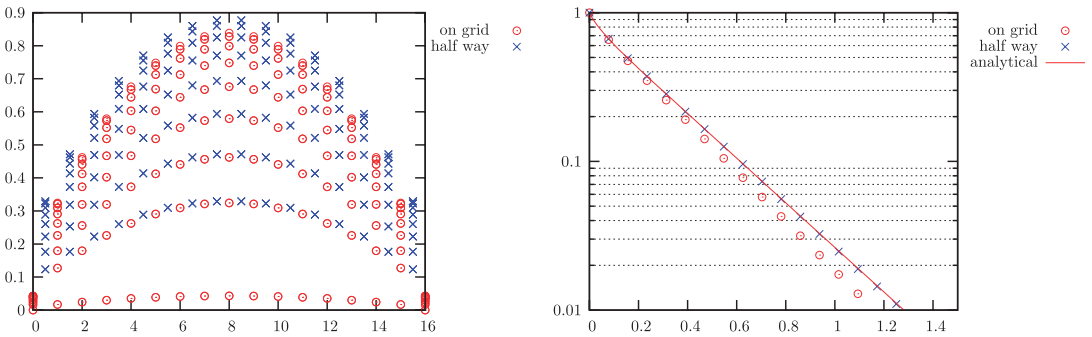

Figure 3. A comparison of two ways of placing the boundary (for the $2DQ5$ grid): (1) on the grid points and (2) half way between grid points. The side length is $L=16\delta_x$. Left: a plot of $\rho(t_1,x,y)$ against the x coordinate. t_1 is chosen such that $\rho(t_1)/\rho(0)\simeq 0.50$. Right: the magnetic signal as a function of time ($\tau=1$) in the two cases and also the corresponding analytical solution.

The L_2 norm for the $2DQ9$ and $2DQ5$ lattice is shown in the upper and lower parts of Figure 4, respectively. From Figure 4 it is clearly seen that the four velocity model converges faster. A fit to the lines in Figure 4 gives a slope of 2 (2.03 for $\gamma=10$ and 1.99 for $\gamma=1$) for the $2DQ5$ lattice. For the $2DQ9$ lattice, the slopes are 1 for $\gamma=1$ and between 1 and 2 for $\gamma=10$ (dependent on τ). In Figure 4, we have also plotted the L_2 norm for different values of the collision parameter τ. The effect of increasing τ is a somewhat less accurate solution for a given lattice size, but the simulation time is shorter. The simulation time scale is inversely proportional to the diffusion constant:

$$t_{\text{sim}}\sim L^2/D=L^2/(C_2(\tau-1/2)) \tag{26}$$

Then for two different values of τ, we have

$$t_{\text{sim}_1}/t_{\text{sim}_2}=(\tau_1-1/2)/(\tau_2-1/2) \tag{27}$$

For $\tau_1=3$ and $\tau_2=1$, $t_{\text{sim}_1}/t_{\text{sim}_2}=5$. This argument can also be used for the simulation time difference by using a $2DQ9$ and $2DQ5$ lattice. Assuming the collision parameter to be the same in the case of the $2DQ5$ and $2DQ9$ lattice, we have $t_{\text{sim}}^{2DQ5}/t_{\text{sim}}^{2DQ9}=D_{2DQ9}/D_{2DQ5}=\frac{3}{2}$, where we have used that $C_{22DQ9}=\frac{3}{4}$ and $C_{22DQ5}=\frac{1}{2}$. The simulation time with the $2DQ5$ lattice is 1.5 times longer, which is a consequence of the fact that the particles on the $2DQ9$ lattice can spread out in eight directions compared with the four directions in the $2DQ5$ lattice. In practice, the simulation takes about the same time in both cases, as more operations need to be performed in the case of the $2DQ9$ lattice. To conclude, in the case of the square the $2DQ5$ lattice performs much better than the $2DQ9$ lattice. The following subsection reveals that this is an effect of the representation of the boundary.

3.3. Test of the boundary condition in the case of an equilateral triangle

In this section, we will discuss effects of the lattice in a more non-trivial case than the square. We have chosen an equilateral triangle [21], see Appendix A, for this purpose. The Robin boundary condition is a boundary value problem where only the combination of the flux and field is known

DOI: 10.1002/fld

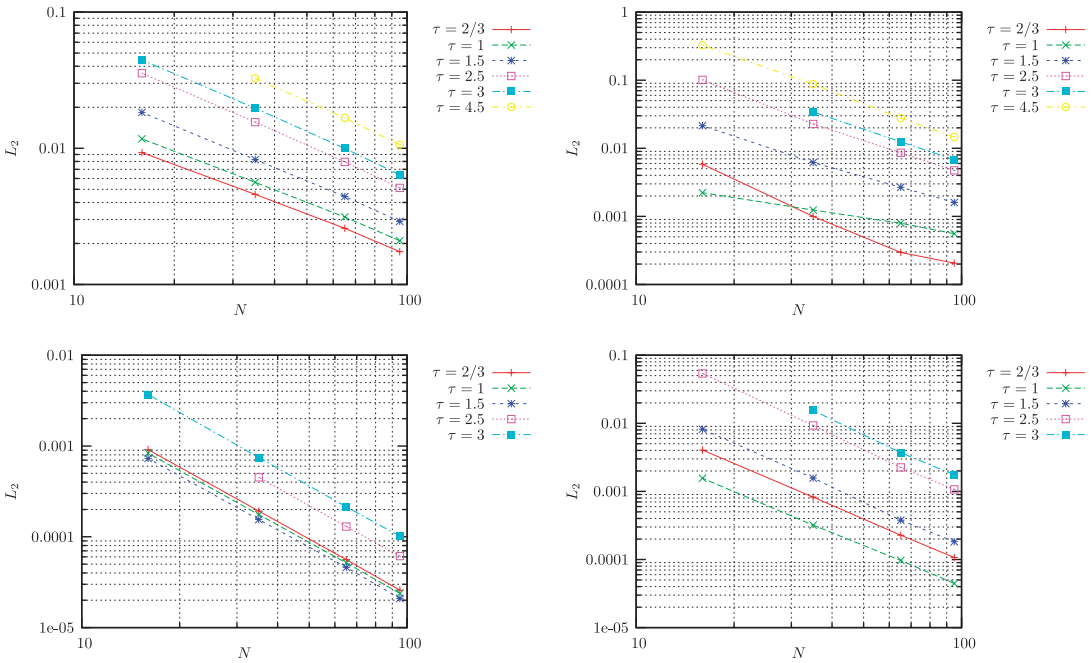

Figure 4. L_2 norm calculated after a time where the magnetic signal is 50% of its original value. Upper-left: L_2 norm for $2DQ9$ and $\gamma = 1$. Upper-right: L_2 norm for $2DQ9$ and $\gamma = 10$. Lower-left: L_2 norm for $2DQ5$ and $\gamma = 1$. Lower-right: L_2 norm for $2DQ5$ and $\gamma = 10$.

at the surface. It is therefore expected that the discretization of the boundary will greatly impact the numerical solution. For simplicity, we compare the magnetic signal not at a given time, but as a function of time i.e. $\rho(t) = \int \rho(x, y, t)\,\mathrm{d}x\,\mathrm{d}y$. From Figure 5, we clearly see that the $2DQ5$ lattice performs much poorer than the $2DQ9$ lattice. Even worse the solution does not converge to the correct solution as the number of lattice points is increased. The explanation for this can be found by studying the analytical solution in more detail. In the limit of low surface effects ($\sigma \to 0$ or $\gamma \to 0$), the analytical solution simplifies (see Appendix A):

$$\rho(t) = \exp\left\{\sigma \frac{S}{V} t\right\} \tag{28}$$

where S and V are the surface and the volume, respectively. The $2DQ5$ lattice does not see a straight line but a stair type of boundary. When representing a straight line with stairs as in Figure 6 one overestimates the surface. In a Dirichlet problem, this would probably not have such a great impact as the value of the field at the surface is known, but in our case the rate at which magnetic signal disappears is proportional to the surface. Consequently, the numerical solution is much more sensitive for an accurate representation of the boundary. By simply counting the side length in Figure 6 we find $44\delta_x$, the correct side length is $3 \times 12\delta_x = 36\delta_x$ for an equilateral triangle. This will give a systematic correction for the surface of $\frac{44}{36} \simeq 1.22$. By correcting the solution obtained for $2DQ5$ lattice by dividing the surface area S with this factor (see Equation (28)), we find the solution shown to the right in Figure 6. Now the numerical solution is much closer to the analytical

DOI: 10.1002/fld

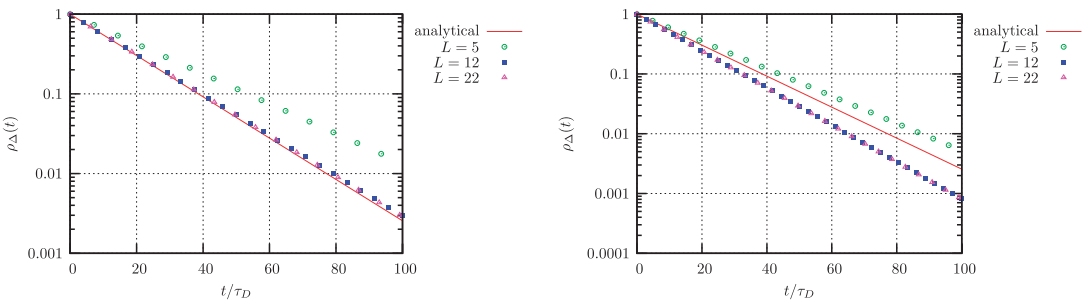

Figure 5. The magnetic signal as a function of time, $\tau=1$ and low surface effect $\gamma=0.01$. Left: $2DQ9$ lattice and right: $2DQ5$ lattice.

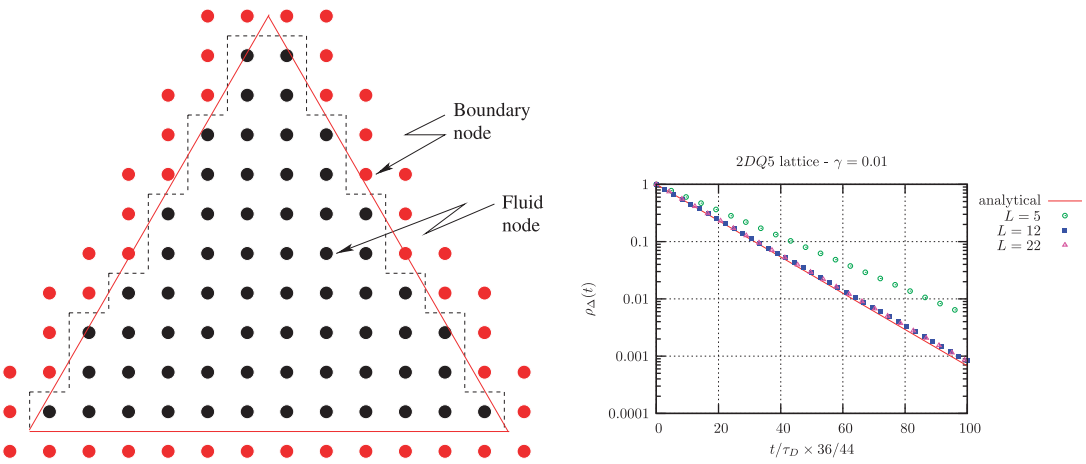

Figure 6. Regular lattice representation of an equilateral triangle with $L=12$. Corrected solution for the $2DQ5$ lattice.

solution. When the surface effect increases (i.e. γ increases), it is not so easy to make any lattice corrections. When $\gamma=1$, the correction is of the order of 11% for the $2DQ5$ lattice; see the left figure in Figure 7. The strength of the $2DQ9$ lattice is clearly seen to the right in Figure 7, where a good match is obtained for a side length as low as $12\delta_x$.

3.4. Comparison with RW algorithm

In this section we compare the LB algorithm for the $2DQ5$ lattice with the RW algorithm [3–8]. In Appendix B, the RW algorithm that we use is derived. The result of the simulations is shown in Figure 8. We use 10^6 random walkers in the simulation. From the figure we see that the LB and the RW algorithms perform well for low surface effects (i.e. low γ). The LB algorithm has more or less the same accuracy for a side length of $5\delta_x$, compared with $10\delta_x$ for the RW algorithm. In the case of high surface effects (i.e. high γ), the number of grid points must be increased in order to get a good accuracy for the RW algorithm. The LB algorithm performs very well in both cases

DOI: 10.1002/fld

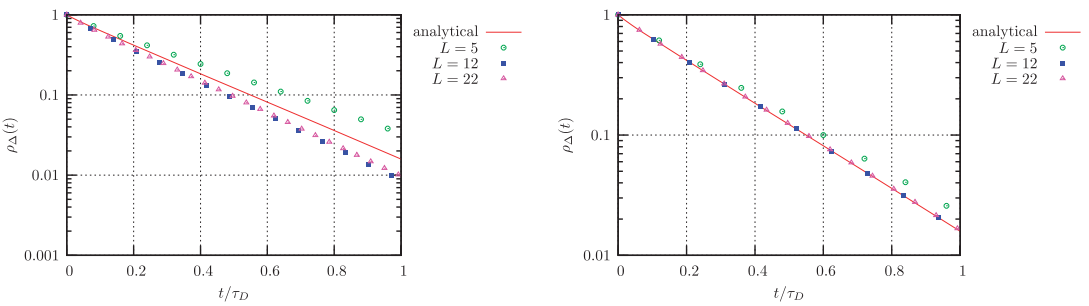

Figure 7. Moderate surface effects $\gamma=1$. Left: $2DQ5$ lattice and right: $2DQ9$ lattice.

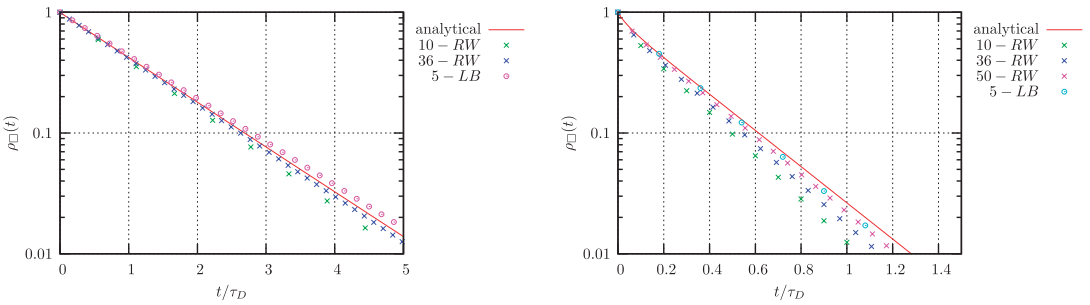

Figure 8. The magnetic signal as a function of time, comparison random walk algorithm and lattice Boltzmann ($\tau=1$). Left: low surface effects $\gamma=1$ and right: high surface effects $\gamma=10$.

with few grid points. The reason for the relative slow convergence of the RW algorithm for high surface effects, compared with the low surface effects, is probably due to the fact that the walkers die faster in this case. In order to get good statistics in the RW simulations, one must average over a high number of walkers. If the walkers die fast (high γ), there will be a lower number at later times and, hence, a poorer statistic.

4. DISCUSSION AND CONCLUSION

We have presented an LB-BGK algorithm for diffusion equation with a Robin boundary condition. We have specialized to the case of a fluid with zero flow velocity. However, if the velocity of the fluid can be ignored at the boundary, the equations presented in Sections 2 and 3 can be used in solving a convective diffusion problem with a Robin boundary condition. We have focused on application to NMR relaxation; the same algorithm can also be used for absorption of chemical components in porous media [14–16]. In [14–16] the expression for the reflected distribution functions was dependent on the collision parameter τ. In this work it is not dependent on τ; see Equations (22) and (24). The justification for this has been done on the basis of comparison with analytical solutions.

DOI: 10.1002/fld

A comparison between a RW-type algorithm and LB has been performed; in the case of a square domain, the LB algorithm performs considerably better than the RW algorithm. The LB algorithm does a better job at low number of grid points, and this is more pronounced at low surface effects.

We have found that the lattice effects are very important. If the boundary is not correctly discretized, it will greatly impact the numerical result. For the $2DQ5$ lattice, we have a perfect match in case of the square, with a quadratic convergence to the analytical solution. In the case of the triangle, the $2DQ5$ lattice has a systematic error of 22%, in the case of low surface effects.

The $2DQ9$ lattice performs well in both cases; from Figure 4 it is evident that the $2DQ9$ lattice only has a linear convergence to the solution. This convergence is slow because the boundary is not optimally discretized by the $2DQ9$ lattice. If one wants to have a fast convergence one needs to have a lattice that approximates the boundary in an accurate manner. For the square, one should use the $2DQ5$ lattice and for the equilateral triangle a hexagonal lattice [21].

The lattice effects are worst for low surface effects ($\gamma \ll 1$) and less important for higher surface effects. This makes it impossible to make any correction for the lattice effects, other than having a very good representation of the geometry. The physical reason why the boundary is less important at higher surface effects is that at low surface effects the spins (or chemical components) diffuse fast and hit the surface many times before they relax (adsorb). Hitting the surface many times means that the diffusing particles are very sensitive to the exact geometry of the surface. As surface effects increase, the particles only hit the surface a couple of times before they disappear.

The important lesson learnt from simulating on a triangular and square domain is that the $2DQ9$ lattice is much less sensitive to discretization errors. Even if we do not have a perfect representation of the geometry, the $2DQ9$ lattice gives a satisfying result. If this algorithm is to be used in ideal geometries, one must be careful to choose a lattice topology that gives a good representation of the boundary. In more complex geometries, one should use the $2DQ9$ lattice as this is less affected by the discretization errors. From the left figure in Figure 5, we see that there is a very good match between the analytical and numerical solution for as few as 12 lattice points. This is important as there is a practical limit in grid size when calculating the numerical solution from a porous media where the number of pores is very large. The boundary condition presented here is symmetric, and it has the same form regardless of the orientation of the wall and, therefore, makes it useful for simulating on complex geometries.

APPENDIX A

A.1. Analytical solutions at zero flow velocity

In order to obtain an analytical solution one uses Green's function method, we express the magnetization, ρ, as (Figure A1)

$$\rho(t) = \int_V \mathrm{d}\mathbf{r}\rho(\mathbf{r}, t) \tag{A1}$$

$$\rho(\mathbf{r}, t) = \int_V \mathrm{d}\mathbf{r}'\chi(\mathbf{r}')G(\mathbf{r}', \mathbf{r}, t) \tag{A2}$$

where $\chi(\mathbf{r}')$ is the initial spin density and $G(\mathbf{r}', \mathbf{r}, t)$ is Green's function. It is defined as the probability for a particle at position $\mathbf{r}'$ at time 0 to diffuse to point $\mathbf{r}$ during a time t. The propagator

DOI: 10.1002/fld

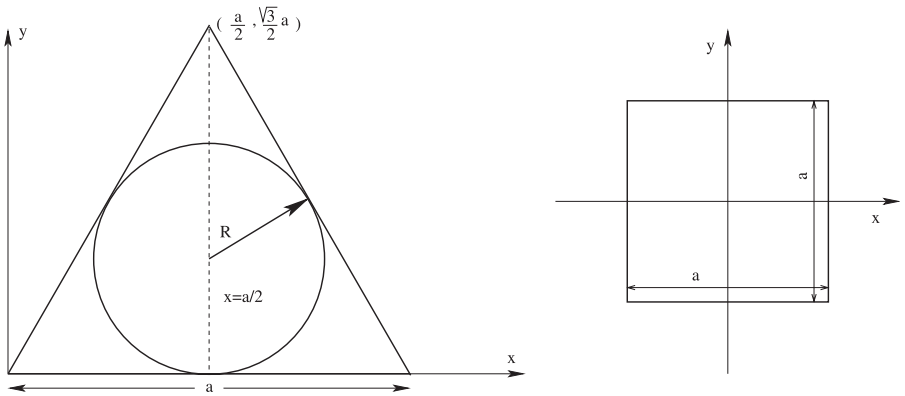

Figure A1. Coordinate system for analytical solutions.

satisfies the diffusion equation at the interior of the pore space:

$$\frac{\partial G(\mathbf{r}|\mathbf{r}';t)}{\partial t} - D\nabla^2 G(\mathbf{r}|\mathbf{r}';t) = 0$$

and

$$G(\mathbf{r}|\mathbf{r}';t)|_{t=0} = \delta(\mathbf{r}-\mathbf{r}') \tag{A3}$$

The boundary condition at the surface $\mathscr{S}$

$$D\hat{\mathbf{n}}\cdot\nabla G(\mathbf{r}|\mathbf{r}';t) + \sigma G(\mathbf{r}|\mathbf{r}';t)|_{\mathbf{r}=\mathscr{S}} = 0 \tag{A4}$$

We use the standard eigenfunction expansion of the propagator:

$$G(\mathbf{r}|\mathbf{r}';t) = \sum_{i=0}^{\infty} \phi_i(\mathbf{r})\phi_i(\mathbf{r}')\mathrm{e}^{-t/T_i} \tag{A5}$$

where $\{\phi_i\}$ are an orthonormal set of eigenfunctions with corresponding eigenvalues T_i. From Equations (A3) and (A4) it then follows:

$$D\nabla^2\phi_i(\mathbf{r}) = -\frac{1}{T_i}\phi_i(\mathbf{r})$$

and

$$D\hat{\mathbf{n}}\cdot\nabla\phi_i(\mathbf{r}) + \sigma\phi(\mathbf{r})|_{\mathbf{r}=\Sigma} = 0 \tag{A6}$$

For a square, the solution is easily found by using the method of separation of variables:

$$\phi(\mathbf{r}') = X(x)Y(y) \tag{A7}$$

DOI: 10.1002/fld

Green's function can then be expressed for a square as

$$
\begin{aligned}
G(x,y|x',y';t) = \sum_{i,j} & \frac{4\xi_1\xi_2}{a^2(\xi_1+\cos\xi_1\sin\xi_1)(\xi_2+\cos\xi_2\sin\xi_2)} \\
& \times \cos\frac{2\xi_1 x'}{a}\cos\frac{2\xi_2 y'}{a}\cos\frac{2\xi_1 x}{a}\cos\frac{2\xi_2 y}{a}\mathrm{e}^{-t/T_i} \\
& \xi_1\tan\xi_1=\gamma/2, \quad \xi_1\in[(2i-1)\pi/2,\pi(2i+1)/2] \\
& \xi_2\tan\xi_2=\gamma/2, \quad \xi_2\in[(2j-1)\pi/2,\pi(2j+1)/2] \\
& \gamma\equiv\sigma a/D \quad \text{and} \quad T_i=\frac{a^2}{D}(\xi_1^2+\xi_2^2)
\end{aligned}
\tag{A8}
$$

For an equilateral triangle, the calculation is a bit more involved, but the result can be expressed [21] as

$$
G(x,y|x',y';t)=\sum_{i=0}^{\infty}\frac{T_i^s(x,y)T_i^s(x',y')}{N_i^{s\,2}}\mathrm{e}^{-t/T_i} \tag{A9}
$$

where

$$
\begin{aligned}
T_i^s(x,y) &= \cos\left[\frac{2\pi\mu}{3R}y-\delta_2\right]+2\cos\left[\frac{\pi\mu}{\sqrt{3}R}(\sqrt{3}R-x)\right]\cos\left[\frac{\pi\mu}{3R}(y-3R)+\delta_2\right] \\
N_i^{s\,2} &= \frac{9\sqrt{3}R^2}{16(\mu\pi)^2}\{8(1+\mu^2\pi^2)-7\cos[2\delta_2]-8\cos[2\mu\pi]-\cos[2\delta_2-4\mu\pi] \\
&\quad +8\cos[2\delta_2-2\mu\pi]+4\mu\pi\sin[2\delta_2]-16\mu\pi\sin[2\delta_2-2\mu\pi]\}
\end{aligned}
\tag{A10}
$$

$$
T_i^{-1}=\frac{4D}{9}\left(\frac{\pi\mu}{R}\right)^2 \tag{A11}
$$

$R=2\sqrt{3}a$ is the radius of the inscribed circle in the equilateral triangle. μ and δ_2 are determined from the boundary condition (17) and it gives rise to the following transcendental equation:

$$
\begin{aligned}
\left[1-\frac{3}{8}\left(\frac{\gamma}{\pi\mu}\right)^2\right]\tan\pi\mu &= \frac{9\gamma}{4\sqrt{3}\pi\mu}, \quad \mu\in\langle i,1+i] \\
\delta_2 &= \tan^{-1}\frac{3\gamma}{4\sqrt{3}\pi\mu} \quad \text{and} \quad \gamma\equiv\sigma a/D
\end{aligned}
\tag{A12}
$$

When Green's function is known, the magnetic signal can be calculated once the initial magnetization is known. For simplicity, we will chose a uniform initial magnetization:

$$
\chi(x,y,0)=\frac{1}{V} \tag{A13}
$$

DOI: 10.1002/fld

where V is the volume. Then we have

$$\rho_\Delta(x,y,t) = -\sum_{i=0}^{\infty} \frac{9\sqrt{3}R^2}{2(\mu\pi)^2 N_i^{s\,2}} T_{ii}^s(x,y)(\cos[\delta_2]-\cos[\delta_2-2\mu\pi]+2\mu\pi\sin[\delta_2])\mathrm{e}^{-t/T_{ii}} \tag{A14}$$

$$\rho_\square(x,y,t) = \sum_{i,j} \frac{4\xi_1\xi_2}{a^2(\xi_1+\cos\xi_1\sin\xi_1)(\xi_2+\cos\xi_2\sin\xi_2)} \times \cos\frac{2\xi_1 x}{a}\cos\frac{2\xi_2 y}{a}\sin\xi_1\sin\xi_2\mathrm{e}^{-t/T_i} \tag{A15}$$

The magnetization as a function of time can then be found by performing the last integration:

$$\rho_\square(t) = \sum_{i=0}^{\infty} \frac{4\sin^2\xi_1\sin^2\xi_2}{\xi_1\xi_2(\xi_1+\cos\xi_1\sin\xi_1)(\xi_2+\cos\xi_2\sin\xi_2)}\mathrm{e}^{-t/T_i} \tag{A16}$$

$$\rho_\Delta(t) = \sum_{i=0}^{\infty} \frac{27\sqrt{3}R^2}{4(\mu\pi)^4 N_i^2}(\cos[\delta_2]-\cos[\delta_2-2\mu\pi]+2\mu\pi\sin[\delta_2])^2\mathrm{e}^{-t/T_i} \tag{A17}$$

Two aspects should be noted regarding the analytical solutions. First, if the surface relaxtivity approaches zero, $\sigma\to 0$, only one mode contributes to the magnetic signal and

$$\rho(t) = \rho(0)\exp\{-t/T\}, \quad \frac{1}{T} = \sigma\frac{S}{V} \tag{A18}$$

where S is the surface area and V the volume of the triangle or the square. This is a special case of the general result obtained by Brownstein and Tarr [1, 2], where they showed that this holds for all kind of geometries. Second, if one introduces a dimensionless time, then

$$t\to\frac{t}{\tau_D}, \quad \tau_D = \left(\frac{V}{S}\right)^2\frac{1}{D} \tag{A19}$$

$\tau_D = a^2/(16D)$, $a^2/(48D)$ for a square and an equilateral triangle, respectively. Then the magnetic signal is only dependent on the value of $\gamma=\sigma a/D$; see (A16) and (A17). Therefore, if one plots the magnetic signal as a function of a rescaled time only then the value of γ needs to be given.

A.2. The RW algorithm

In order for the paper to be self-contained, we present the RW algorithm on a regular grid with four directions [3–8]. By applying a set of rules for random walkers placed on the grid, we can derive the diffusion equation in the continuum limit.

Random walkers are placed at random at a lattice point in the simulation domain. The number of random walkers at an interior point (x, y) (see Figure A2) when the clock advance one step τ is equal to the incoming flux from neighboring points:

$$\rho(x,y,t+\tau)-\rho(x,y,t) = \tfrac{1}{4}[\rho(x+\varepsilon,y,t)-\rho(x,y,t)+\rho(x-\varepsilon,y,t)-\rho(x,y,t) + \rho(x,y+\varepsilon,t)-\rho(x,y,t)+\rho(x,y-\varepsilon,t)-\rho(x,y,t)] \tag{A20}$$

DOI: 10.1002/fld

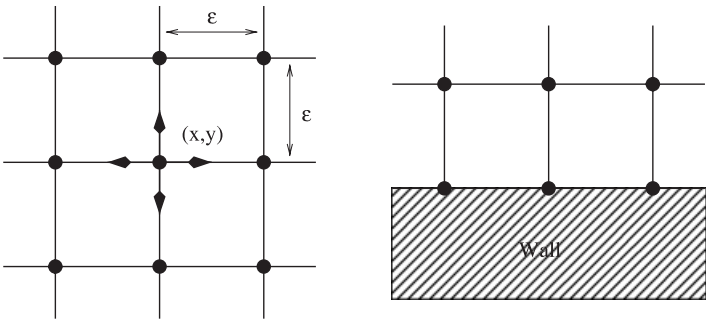

Figure A2. Left: regular grid used for random walk simulations, inside the simulation domain. Right: points close to the boundary.

The factor $\frac{1}{4}$ in front is the probability that a walker takes a step in one of the four directions. Dividing this equation by τ, we find after some rearrangement the following:

$$\frac{\rho(x,y,t+\tau)-\rho(x,y,t)}{\tau}=\frac{1}{4}\frac{\varepsilon^2}{\tau}\left[\frac{\rho(x+\varepsilon,y,t)-2\rho(x,y,t)+\rho(x-\varepsilon,y,t)}{\varepsilon^2}\right. \tag{A21}$$

$$\left.+\frac{\rho(x,y+\varepsilon,t)-2\rho(x,y,t)+\rho(x,y-\varepsilon,t)}{\varepsilon^2}\right] \tag{A22}$$

The lattice spacing is given by ε. Taking the limit $\tau\to 0$, $\varepsilon\to 0$:

$$\frac{\partial\rho(x,y,t)}{\partial t}-D\nabla^2\rho(x,y,t)=0 \tag{A23}$$

where

$$D\equiv\frac{\varepsilon^2}{4\tau} \tag{A24}$$

The boundary condition can be derived in a similar way. We introduce a probability of 'dying,' $\zeta\in[0,1]$, when a walker hits the wall. For a wall parallel to the x-axis (see Figure A2), the number of random walkers at a boundary point is equal to the flux from neighboring points:

$$\varepsilon\frac{\rho(x,y,t+\tau)-\rho(x,y,t)}{\tau}=\varepsilon\frac{\varepsilon^2}{4\tau}\left[\frac{\rho(x+\varepsilon,y,t)-2\rho(x,y,t)+\rho(x-\varepsilon,y,t)}{\varepsilon^2}\right] \tag{A25}$$

$$+\frac{\varepsilon^2}{4\tau}\frac{\rho(x,y-\varepsilon,t)-\rho(x,y,t)}{\varepsilon}-\frac{\zeta\varepsilon}{4\tau}\rho(x,y,t) \tag{A26}$$

We have multiplied by ε/τ and sorted out the diffusion constant $\varepsilon^2/4\tau$, which approaches a constant when $\varepsilon,\tau,\to 0$. Thus, in the limit $\varepsilon,\tau,\to 0$, we find

$$D\mathbf{n}_y\cdot\nabla\rho(x,y,t)+\sigma\rho(x,y,t)=0 \tag{A27}$$

where

$$\sigma\equiv\frac{\zeta\varepsilon}{4\tau} \tag{A28}$$

where $\mathbf{n}_y$ is the unit vector in the y-direction.

DOI: 10.1002/fld

ACKNOWLEDGEMENTS

The authors acknowledge ConocoPhillips and the Ekofisk Coventurers, including TOTAL, ENI, Hydro, Statoil and Petoro, for financing the work and for the permission to publish this paper from the research center COREC.

REFERENCES

1. Brownstein K, Tarr C. Spin–lattice relaxation in a system governed by diffusion. *Journal of Magnetic Resonance* 1977; **26**:17–24.
2. Brownstein K, Tarr C. Importance of classical diffusion in NMR studies of water in biological cells. *Physical Review* 1979; **A**(19):2446–2453.
3. Wilkinson D, Johnson D, Schwartz L. Nuclear magnetic relaxation in porous media: the role of the mean lifetime $\tau(\rho, D)$. *Physical Review B* 1991; **44**:4960–4973.
4. Mitra P, Sen P, Schwartz L. Short time behavior of the diffusion coefficient as a geometrical probe of porous media pore geometries. *Physical Review B* 1993; **47**:8565–8574.
5. Mendelson K. Continuum and random-walk models of magnetic relaxation in porous media. *Physical Review B* 1993; **47**:1081–1083.
6. Mendelson K. Percolation model of nuclear magnetic relaxation in porous media. *Physical Review B* 1990; **41**:562–567.
7. Bergman D, Dunn K, Schwartz L, Mitra P. Self-diffusion in a periodic porous medium: a comparison of different approaches. *Physical Review E* 1990; **51**:3393–3400.
8. Toumelin E, Torres-Verdin C, Chen S. Modeling of multiple echo-time NMR measurements for complex pore geometries and multiphase saturations. *2002 SPE Annual Technical Conference and Exhibition*, San Antonio, 29 September–2 October 2002; SPE 85635.
9. Inamuro T, Yoshino M, Inoue H, Mizuno R, Ogino F. A lattice Boltzmann method for a binary miscible fluid mixture and its application to a heat-transfer problem. *Journal of Computational Physics* 2002; **179**:201–215.
10. Barrios G, Rechtman R, Rojas J, Tovar R. The lattice Boltzmann equation for natural convection in a two-dimensional cavity with a partially heated wall. *Journal of Fluid Mechanics* 2005; **522**:91–100.
11. Zhaoli G, Baochang S, Chuguang Z. A coupled lattice BGK model for the Boussinesq equations. *International Journal for Numerical Methods in Fluids* 2002; **39**:325–342.
12. Mishra S, Roy H. Solving transient conduction and radiation heat transfer problems using the lattice Boltzmann method and the finite volume method. *Journal of Computational Physics* 2006. DOI: 10.1016/j.jcp.2006.08.021.
13. Mishra S, Lankadasu A, Beronov K. Application of the lattice Boltzmann method for solving the energy equation of a 2-D transient conduction–radiation problem. *International Journal of Heat and Mass Transfer* 2005; **48**:3648–3659.
14. Dawson S, Chen S, Doolen G. Lattice Boltzmann computations for reaction–diffusion equations. *Journal of Chemical Physics* 1993; **15**:1514–1523.
15. Kang Q, Zhang D, Chen S, He X. Lattice Boltzmann simulation of chemical dissolution in porous media. *Physical Review E* 2002; **65**:036318.
16. Kang Q, Zhang D, Chen S. Simulation of dissolution and precipitation in porous media. *Journal of Geophysical Research* 2003; **108**(B10):2505.
17. Shan X, Doolen G. Diffusion in a multicomponent lattice Boltzmann equation model. *Physical Review E* 1996; **54**:3614–3620.
18. Shan X, Hudong C. Lattice Boltzmann model for simulating flows with multiple phases and components. *Physical Review E* 1993; **47**:1815–1819.
19. Succi S. *The Lattice Boltzmann Equation for Fluid Dynamics and Beyond*. Oxford University Press: Oxford, 2001.
20. Wolf-Gladrow D. A lattice Boltzmann equation for diffusion. *Journal of Statistical Physics* 1995; **79**:1023–1032.
21. Finjord J, Hiorth A, a Lad U, Skjæveland S. NMR for equilateral triangular geometry under conditions of surface relaxivity—analytical and random walk solution. *Transport in Porous Media* 2006, online.